

# Geometrical and optical analysis of small-sized parabolic trough collector using ray tracing tool SolTrace

RAMAN KUMAR SINGH\*  
PRAKASH CHANDRA

National Institute of Technology Patna, Department of Mechanical Engineering, Bihar 800005, India

**Abstract** The present work is aimed at geometrical optimization and optical analysis of a small-sized parabolic trough collector (PTC). Improving the performance of parabolic trough collectors can greatly justify the use of solar energy. An optimized curvature geometry, the location of the absorber tube, and the heat flux distribution along the circumference of the absorber tube are major features in the geometric optimization and optical modelling of parabolic trough collectors. Rim angle, aperture width, the diameter of the absorber tube, receiver position, and the optimum value of heat flux are the major parameters considered in this work for geometrical and optical analysis. The Monte Carlo ray tracing method has been adopted for analysis. The non-uniform heat flux distribution profile obtained from optical analysis of the proposed parabolic trough collector has been compared with the profile available in the literature, and good agreement has been obtained, which proves the feasibility and reliability of the model and method used for this study. An experimental new small-sized parabolic trough collector has been fabricated for the optimized rim angle of 90 deg after a successful laser light feasibility test. The effect of the absorber tube position along the optical axis on the heat flux profile was analysed and found to be substantial. Furthermore, the sensitivity analysis of the parabolic trough collector using the software applied has been discussed separately.

**Keywords:** Parabolic trough collector; SolTrace; Monte Carlo ray tracing method; Non-uniform heat flux distribution; Optical analysis; Geometrical analysis

---

\*Corresponding Author. Email: [ramanks.phd19.me@nitp.ac.in](mailto:ramanks.phd19.me@nitp.ac.in)

## Nomenclature

$A_s$	–	surface area, m <sup>2</sup>
$A_p$	–	aperture area, m <sup>2</sup>
CR	–	concentration ratio
DNI	–	direct normal irradiation, W/m <sup>2</sup>
$f$	–	focal length, m
$H$	–	height of the trough, m
$L$	–	length of the trough, m
LCR	–	local concentration ratio
$l$	–	length of the absorber tube, m
$d_o$	–	outer diameter of the absorber tube, m
$r_r$	–	rim radius, m
$W_a$	–	aperture width, m
$x, y$	–	Cartesian coordinates, m
$q$	–	local heat flux, W/m <sup>2</sup>

## Greek symbols

$\alpha_D$	–	acceptance angle, deg
$\phi_r$	–	rim angle, deg

## Acronyms

CFD	–	computational fluid dynamics
CSHFD	–	circumferential solar heat flux distribution
CSP	–	concentrated solar power
CTG	–	circumferential temperature gradient
MCRT	–	Monte Carlo ray tracing
PTC	–	parabolic trough collector
SEGS	–	solar energy generating system

## 1 Introduction

The parabolic trough collector (PTC) is a line-focused type of concentrated solar power (CSP) technology that is prominently used due to its wide temperature range (up to 400°C). The reflector and absorber tubes are two major components of PTC. A reflector concentrates incoming beam radiation at the focus of the aperture at which the absorber tube is kept so that the heat transfer fluid (HTF) passing through it gets heated [1, 2]. Optical performance significantly influences PTC's overall efficiency. By using the method of ray tracing, the optimal configuration of the collector with maximum performance can be obtained. The thermal performance of PTC systems depends upon optical efficiency, which is significantly influenced by the geometry of the collector, heat flux intensity distribution along the

absorber tube circumference, the location of the absorber tube, etc. Various numerical and experimental analyses have been carried out by numerous researchers to investigate the heat flux distribution around the absorber surface of PTC and other CSP technologies.

Wang [3] conducted a review study related to slope error in reflector surface and sun shape using six different optical modelling tools: SolTrace, Tonatiuh, Solar PILOT, Tracer, Solstice, and Heliosim. Mwesigye *et al.* [4] estimated the heat flux profile on the receiver tube surface of PTC using Monte Carlo ray tracing (MCRT) and coupled it to computational fluid dynamics (CFD) for heat transfer analysis. Particularly, they analysed rates of entropy generation at a range of rim angles, concentration ratios, and temperatures of flowing fluid.

Many times, the optical efficiency of the PTC system does not reach expectations due to geometrical and optical faults such as receiver position inaccuracy, misalignment, slope, and profile error, among others. It is important to design by figuring out what these errors are and what they mean for how well PTC works. Donga *et al.* [5] studied the influence of receiver location on the optical and thermal performance of a PTC. The simulation was carried out by coupling MCRT heat flux distribution data with CFD. They found that the error in receiver position had a significant impact on thermal performance and the heat flux profile. Zhao *et al.* [6] simulated heat flux distribution along the circumference of absorber tubes by combining coordinate transformation with the MCRT method. They reported the substantial effects of inaccuracies in receiver position, tracking errors, geometrical concentration ratios, and incident angle on the solar heat flux distribution profile. The error becomes larger with an increase in incident angle and a decrease in geometrical concentration ratios. Treadwell examined the effects of receiver location errors in the lateral direction from the focus [7]. When the receiver position was shifted along the lateral  $y$ -direction by  $\pm 10\%$  of its diameter from the focus, no major change in the performance of the PTC was detected. He also recommended that the receiver tube's diameter be expanded to compensate for misalignment without compromising the PTC's performance significantly. Treadwell and Grandjean said that the receiver positioning error affected the PTC's annual performance, depending on how much the receiver was moved [8]. The above-mentioned literature shows that the receiver position error has a considerable effect on the optical efficiency of the PTC and the heat flux distribution throughout the circumference of the absorber tube, and hence on the thermal performance of the PTC system.

The generation of circumferential solar heat flux distribution (CSHFD) is essential in concentrating solar collectors since it is one of the boundary conditions for the PTC receivers' thermal analysis. Various works from the past are available; a few of them have been discussed here. Ghomrassi analysed numerically the thermal performance of the PTC receiver tube for different diameters by coupling CSHFD obtained in SolTrace software to CFD [9]. Jeter proposed a semi-finite analytical approach for evaluating the CSHFD of the PTC receiver [10]. Wang *et al.* [11] investigated the thermal performance of the PTC system numerically by the finite element method (FEM). Solar flux densities are evaluated by using the solar ray tracing method. Cheng *et al.* [12] investigated the thermal performance of the PTC receiver by combining MCRT with the finite volume method (FVM) and compared their findings with the experimental results of Dudley *et al.* [13]. It was found that the numerical results were quite close to the experimental results. Among other techniques, the MCRT method is extensively used for obtaining focused solar heat flux distribution [5, 6, 9, 11, 12, 14].

From the above discussion, it is clear that for the efficient functioning of PTC systems, the optimised collector geometry, the optical model for concentrated heat flux distribution, and the correct location of the absorber tube are crucial, among other factors. Aperture width, focal length, and rim angle are the parameters that define the size and curvature of a parabolic trough. The rim angle is a single parameter having the capability to define the cross-section of the parabolic trough [15, 16]. Since some smaller and larger rim angles are not good for a reliable PTC, this study gives an optimal rim angle for a new small-sized PTC based on the average and peak values of CSHFD over the absorber tube. More heterogeneous heat flux densities around the circumference of the absorber tube may result in a higher circumferential temperature gradient (CTG), increased thermal stress and strain, damaging the receiver tube and reducing system stability and safety. The impacts of the receiver dislocation from the focus point as well as the sensitivity analysis of the PTC have also been discussed.

## 2 Numerical simulation for design optimization and fabrication of parabolic trough collector

In this section, the numerical modelling of a new small-sized parabolic trough collector and fabrication of a laboratory-scale experimental setup for an indoor experiment have been discussed. In this work, the two major

components of PTC, namely the reflector and absorber, were analysed. Other components, such as the sun tracking mechanism, the glass cover, the heat transfer fluid (HTF), and so on, are irrelevant in this study.

## 2.1 Consideration of design parameters

To define the physical structure of a parabolic trough, there are mainly four geometric parameters: trough length, aperture width, rim angle, and focal length. The size of the absorber tube can be determined by its diameter and length. The two dimensional (2D) cross-sectional view in Fig. 1 depicts critical elements for designing a new small-size PTC. The length of the trough or collector has been determined (1 m) based on prior work related to small-sized PTC, which reported the length of the collector in the range of 1–3 m [17–20]. The lower the aperture width of the trough, the shorter the geometric factor, resulting in greater optical efficiency. For a particular absorber diameter, however, the concentration ratio reduces as the aperture width lowers, resulting in large thermal losses. Kalogirou *et al.* [21] proposed that the aperture width be reduced to a length ratio of 0.64 after aperture width optimization to achieve the goal of having a small geometric factor and a high concentration ratio. Based on the above literature, we can figure out that the aperture width is 0.64 m for the analysis of the present work.

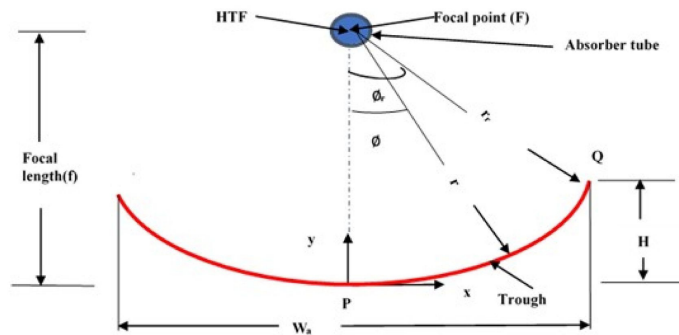


Figure 1: 2D sectional view of present PTC.

One of the critical criteria for the proper operation of any PTC system is the selection of the optimum rim angle [16]. A ray tracing software based on the MCRT algorithm has been adopted for analysing the effect of different rim angles on the concentrated heat flux and selecting the optimum one. The parameters of PTC that have been used in the analysis of CSHFD are listed in Table 1.

Table 1: Parameters of the parabolic trough collector used in the circumferential solar heat flux distribution analysis.

Parameters	Units	Numerical value
Collector length	mm	1000
Aperture width	mm	640
Absorber tube outer diameter	mm	21
Absorber tube inner diameter	mm	19
Absorber tube length	mm	1000
Direct normal irradiance	W/m <sup>2</sup>	1000
Concentration ratio	–	9.38
Reflectivity of concentrator	–	0.88
Absorptivity of the absorber tube	–	0.95
Slope error concentrator	mrad	2
Specularity error of concentrator	mrad	0.5
Sun shape (pillbox)	mrad	4.65
Desired number of ray interaction	–	10 <sup>6</sup>
Maximum number of generated sun rays	–	10 <sup>8</sup>

The analysis has been carried out for a rim angle ranging within 30–130 deg, with a gap of 10 deg to obtain the maximum collection of solar heat flux for a non-ideal concentrator, having the slope and specularity errors mentioned in Table 1.

As the rim angle decreases, the focal length increases, and concentrated heat flux falls on a very small region of the bottom outer surface of the absorber tube while the rest of the tube receives direct normal irradiation (DNI). In this case, the peak value of heat flux (51.3 kW/m<sup>2</sup>) is very high, 51.3 times the DNI (1 kW/m<sup>2</sup>), which can cause thermal stress and damage to the absorber tube due to the high CTG. In Fig. 2, the effect of one of the smaller rim angles (30 deg) on concentrated heat flux density is shown through a ray-intersection plot, contour plot and surface plot.

As the rim angle increases, the focal length reduces, and the reflected radiations from the outer portion of the concentrator travel a relatively greater distance. In this case, the outer part of the reflector also contributes less to reflection. Also, it is clear from Fig. 3 that as the rim angle increases, the intensity of heat flux decreases (16.8 kW/m<sup>2</sup>). Large rim angles are also restricted due to economic constraints and are practically uncomfortable and difficult to handle. Figure 3 depicts the effect of one of the larger rim angles (130 deg) on heat flux distribution.

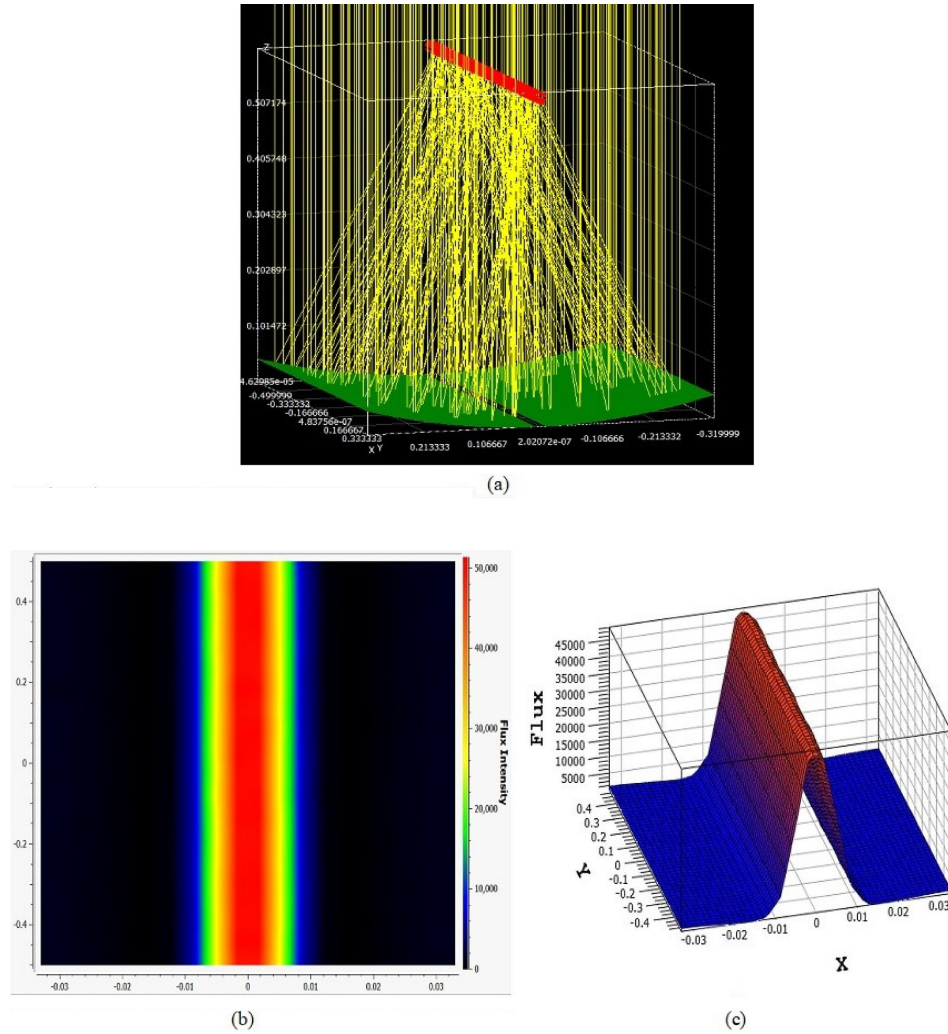
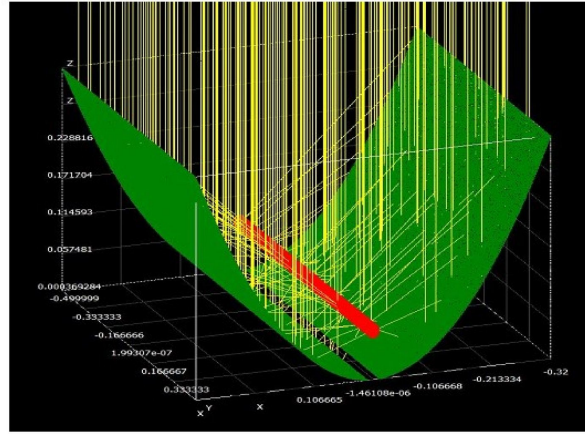


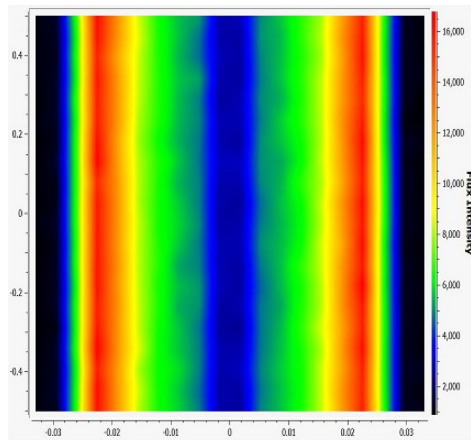
Figure 2: Effect of small rim angle (30 deg) on heat flux: (a) ray intersection plot, (b) contour plot, (c) surface plot.

As it follows from the above discussion, due to some reasons, a range of smaller and larger rim angles are not suitable for a reliable PTC. In the third case, a medium range of rim angles (90 deg) has been taken for analysing its effect on heat flux intensity, which is shown in Fig. 4.

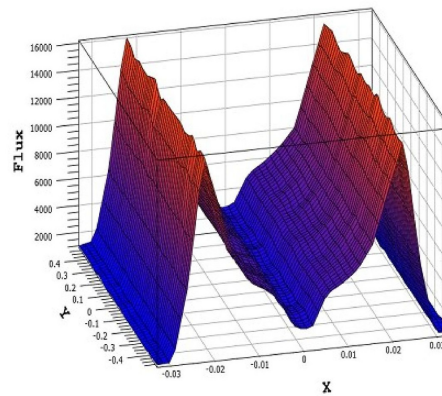
In the case of a 90-degree rim angle, the peak value of heat flux is  $19.4 \text{ kW/m}^2$ , which can be seen in the contour and surface plot in Fig. 4.



(a)



(b)

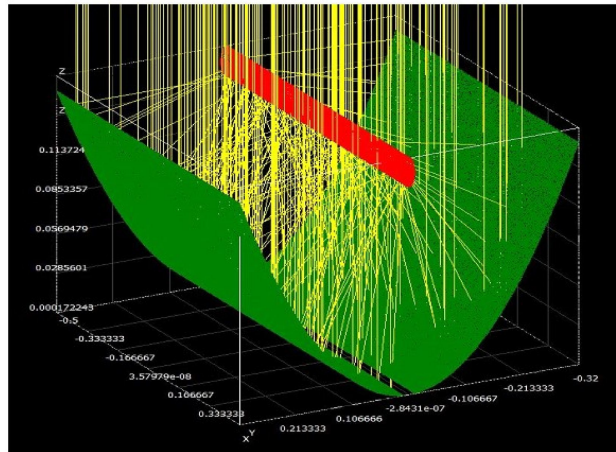


(c)

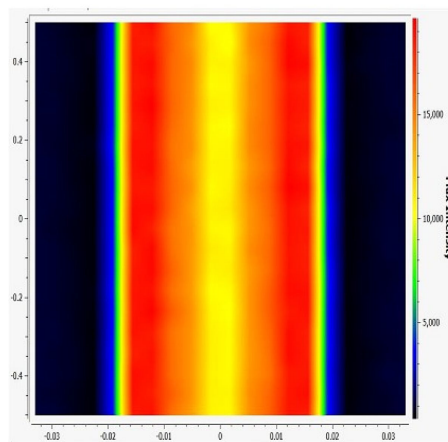
Figure 3: Effect of larger rim angle (130 deg) on heat flux intensity: (a) ray-intersection plot, (b) contour plot, (c) surface plot.

For ease of analysis, the rest of the rim angle range (30–130 deg) and its effect on heat flux intensity have been tabulated in Table 2.

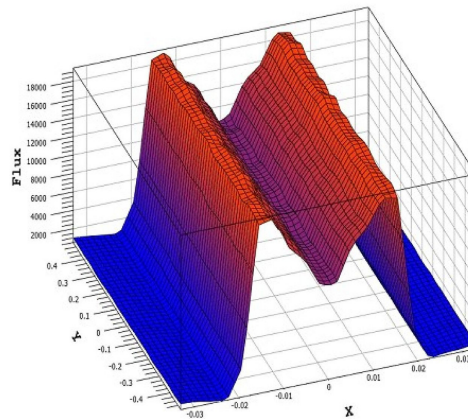
Table 2 shows that the optimum value of average heat flux for a 90-degree rim angle is  $8.58 \text{ kW/m}^2$ , while smaller rim angles of 30 deg and larger rim angles of 130 deg have relatively very high ( $51.3 \text{ kW/m}^2$ ) and poor values ( $16.85 \text{ kW/m}^2$ ) of peak heat flux, respectively, in comparison to  $19.44 \text{ kW/m}^2$  of peak heat flux for a 90-degree rim angle.



(a)



(b)



(c)

Figure 4: Effect of medium range rim angle (90 deg): (a) ray-intersection plot, (b) contour plot, (c) surface plot.

Furthermore, the ideal value of the rim angle for proper operation of the PTC system is 70–110 deg [16], which is satisfied by the result given in Table 2. Table 2 shows that the simulated values of peak and average heat flux for 70–110 deg of rim angle do not vary much. A 90-degree rim angle is most practically employed in PTC with a circular absorber tube, according to Jeter [10]. The above discussion proves that the MCRT method used

Table 2: Comparative analysis of heat flux density for different values of rim angle.

Rim angle (deg)	Peak heat flux (kW/m <sup>2</sup> )	Uncertainty in peak heat flux (%)	Average heat flux (kW/m <sup>2</sup> )	Uncertainty in average heat flux (%)
30	51.3	±0.86	8.55	±0.07
40	35.65	±1.04	8.56	±0.07
50	30.78	±1.12	8.56	±0.07
60	25.86	±1.2	8.57	±0.07
70	23.54	±1.2	8.56	±0.07
80	22.26	±1.32	8.56	±0.07
90	19.44	±1.4	8.58	±0.07
100	20.42	±1.37	8.57	±0.07
110	19.93	±1.39	8.56	±0.07
120	19.81	±1.39	8.55	±0.07
130	16.85	±1.51	6.52	±0.07

in this work is viable and the numerical findings obtained are reliable. So, a 90-degree rim angle is what we have selected for further numerical analysis and the fabrication of an experimental setup.

## 2.2 Data reduction

The different geometrical parameters are discussed mathematically as follows. The aperture of the parabolic trough collector is represented by the parabola equation [22, 23]:

$$y = \frac{x^2}{4f}, \quad (1)$$

where  $x$  and  $y$  are Cartesian coordinates and  $f$  is the focal length of the parabola.

The following is the relationship between focal length, aperture width ( $W_a$ ), and rim angle ( $\phi_r$ ):

$$f = \frac{W_a}{4 \tan \frac{\phi_r}{2}}. \quad (2)$$

The minimum theoretical outer diameter of the absorber tube that can intercept all the reflected DNI is given by the relation as follows [24, 25]:

$$d_o = 2r_r \sin \frac{\alpha_D}{2}, \quad (3)$$

where  $r_r$  is the radius of the rim which can be calculated from the relation [1, 26]

$$r_r = \frac{2f}{1 + \cos \phi_r}. \quad (4)$$

Parameter  $\alpha_D$  is the acceptance angle for maximum concentration and its value is taken as  $0.53^\circ$  [27].

By using Eqs. (3) and (4) for a 90-degree rim angle, we get a minimum theoretical outer diameter of 2.96 mm for the absorber tube. However, due to geometrical imperfections, misalignments, and other constraints, it is difficult to use the theoretically designed diameter for experimental analysis. In this study, we used an absorber tube with an inner diameter of 19 mm and an outer diameter of 21 mm, which is within the range of diameters used by many researchers to investigate small-sized PTC.

The height of the parabolic trough can be obtained by putting  $x = \frac{W_a}{2}$  and  $y = H$  in Eq. (1), which finally gives

$$H = \frac{W_a^2}{16f}. \quad (5)$$

The surface area ( $A_s$ ) of the reflector is given by the relationship [17]

$$A_s = \left[ \frac{W_a}{2} \sqrt{1 + \frac{W_a^2}{16f^2}} + 2f \ln \left( \frac{W_a}{4f} + \sqrt{1 + \frac{W_a^2}{16f^2}} \right) \right] l, \quad (6)$$

where  $l$  is the length of the parabolic trough.

Another important geometrical parameter for focusing type of solar collector is the concentration ratio which is given as

$$\text{CR} = \frac{\text{Effective aperture area}}{\text{Absorber tube surface area}} = \frac{(W_a - d_o)l}{\pi d_o L}, \quad (7)$$

where  $L$  is the length of the absorber tube.

### 2.3 Design methodology for a new parabolic trough collector

The flow chart of the design methodology and the fabrication process for a new small-sized PTC is shown step by step in Fig. 5.

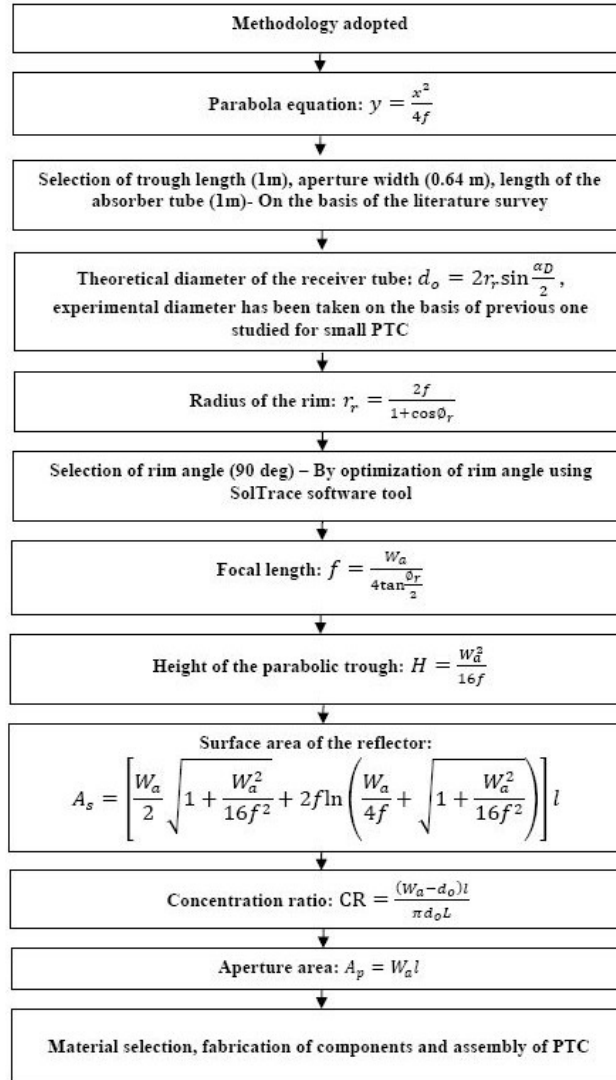


Figure 5: Flow chart for design methodology and fabrication of a new PTC.

## 2.4 Experimental design and fabrication of a parabolic trough collector

This section deals with the experimental process adopted for the design and fabrication of the PTC. First, a laser light test for the design of the curvature of the PTC has been done to determine the feasibility of the technique.

After that, an experimental trough with the dimensions shown in Table 1, including an optimized rim angle of 90 deg and, correspondingly, a value of the focal length of 160 mm calculated using Eq. (2), was fabricated for the further study.

### 2.4.1 Laser light test

This test has been performed for a smaller dimension of the parabola, for the feasibility test of the procedure, and for the ease of conducting the test. The materials and parameters used in the test are summarized in Table 3. Later, this technique was used to create actual troughs for experimentation. Their dimensions are given in Table 4.

Table 3: Parameters and material used for laser light test.

Parameters and material used	Dimensions/Property
Width of aperture	200 mm
Focal length of the parabolic aperture	50 mm
Rim angle	90 deg
Laser light	635 nm
Chrome sheet (reflector) – reflectivity	0.88
Drawing sheet	–

Table 4: Description of the components, materials and its dimensions used in the fabrication of PTC.

Components	Material	Dimension
End aperture of trough	Plywood	Width of aperture: 640 mm
Trough	Galvanised sheet	Length: 1000 mm, width: 640 mm
Absorber tube	Copper	$d_i = 19$ mm, $d_o = 21$ mm
Solar reflector film	Chrome sticker	Reflectivity: 0.88
Focal length	–	160 mm
Rim angle	–	90 deg

In this test, a 635 mm laser light was used as the light source, and a drawing sheet of 1 mm thickness has been shaped into a parabolic curve according to the coordinate points marked on the sheet, obtained by Eq. (1) for the parabola and the parabola calculator 2.0 software [28]. A chrome sheet adhered to the parabolic-shaped sheet was used to reflect the laser light

that fell on it. We can see in Fig. 6 that the laser light, after reflection from the parabolic-shaped reflector, exactly passes through the focal point made at 50 mm focal length, corresponding to a 90-degree rim angle, which proves the feasibility of the test. Sixteen segment coordinate points for designing an accurate parabolic curve have been obtained from the parabola calculator, as shown in Fig. 7. For a 50-mm focal length, the same coordinate points can also be obtained by using the parabola equation (Eq. (1)).

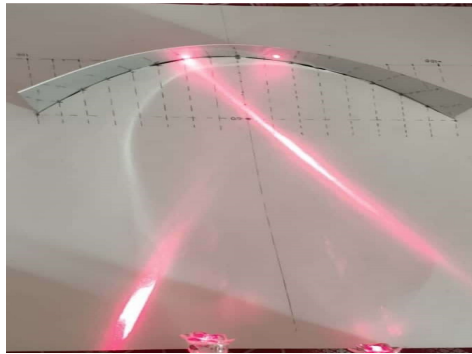


Figure 6: Experimental view of laser light test.

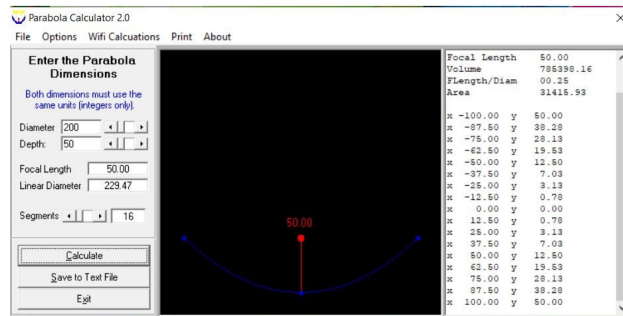


Figure 7: Snap of the parabolic curve and coordinate points in Parabola Calculator 2.0 software [28].

#### 2.4.2 Fabrication of experimental parabolic trough collector

After a successful feasibility test of the laser light, the same procedure was used for the fabrication of experimental PTC, as shown in Fig. 8. Table 4 lists the materials and dimensions used in the fabrication of experimental PTC.

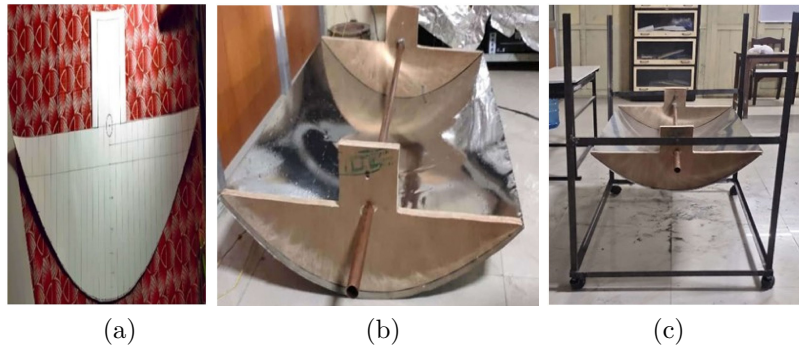


Figure 8: Experimental view of (a) parabolic aperture drawn on the sheet, (b) trough with absorber tube, (c) parabolic trough collector with supporting frame.

### 3 Methodology for heat flux distribution analysis using SolTrace software

The CSHFD analysis with SolTrace is carried out in the steps depicted in flow chart (Fig. 9). It is based on an optical interaction technique that uses the ray tracing method. The programme generates the scatter plot, surface plot (3D), and contour plot (2D) for the heat flux distribution profile on the circumference of the PTC absorber [29]. The first step to analysing the ray tracing is to define the sun's shape and sun position. There are three options available to define the shape of the sun, namely pillbox, Gaussian and user-defined distributions, while the position of the sun is defined either

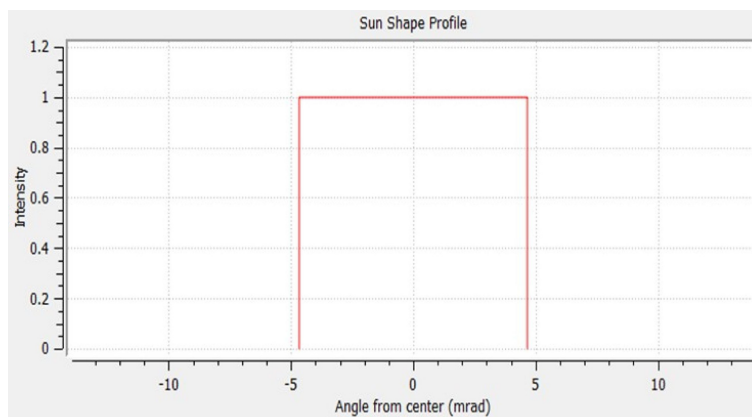


Figure 9: Flow chart of CSHFD analysis using SolTrace software version 2012.7.9.

by the global coordinate system or by defining the latitude, day and solar hour of a particular place. In the present analysis, the sun's shape is defined as a pillbox distribution with a half-angle width of 4.65 mrad as shown in Fig. 10 [11, 29, 30], and the sun position is defined by the global coordinate system. The next step is setting the optical properties of the concentrator and absorber tube as shown in Fig. 9. After defining the optical properties,

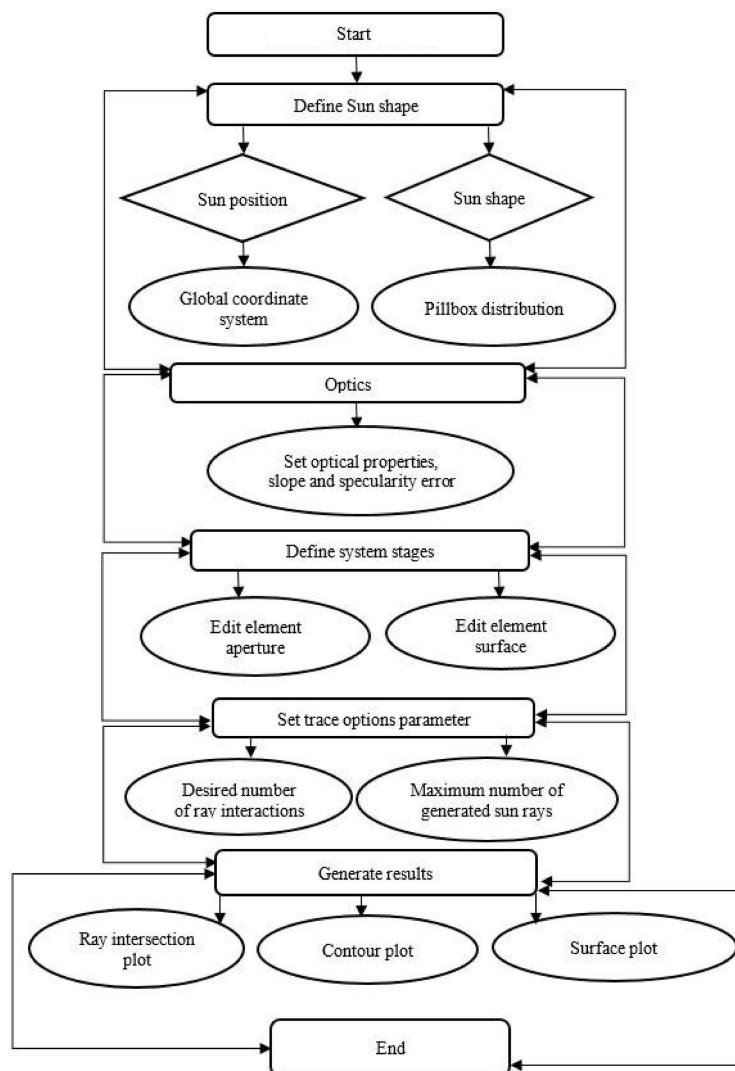


Figure 10: Pillbox sun shape profile.

the geometry of the system was developed by setting stage properties and defining the element aperture and element surface. The desired number of ray interactions of  $10^6$  and a maximum number of generated rays of  $10^8$  have been employed in the trace options parameter to obtain an accurate heat flux profile and save computational time [5]. During simulations, it has been seen that the value of heat flux changes significantly between runs when the desired number of ray interaction values is less than  $10^6$ . A constant value of DNI  $1000 \text{ W/m}^2$  is employed for the simulation. The sun's rays first strike the absorber and concentrator, and the reflected rays from the concentrator fall on the absorber and are absorbed by it.

## 4 Results and discussion

### 4.1 Discussion on non-uniform heat flux profile

Figure 11 shows the surface plot of heat flux distribution along the outer periphery of the absorber tube. The surface plot actually shows the heat flux distribution on the unwrapped absorber tube, varying from 0–360 deg from left to right, where 0 deg and 180 deg stand for the top and bottom positions of the absorber tube, as illustrated in Fig. 12c. As shown in Fig. 11,

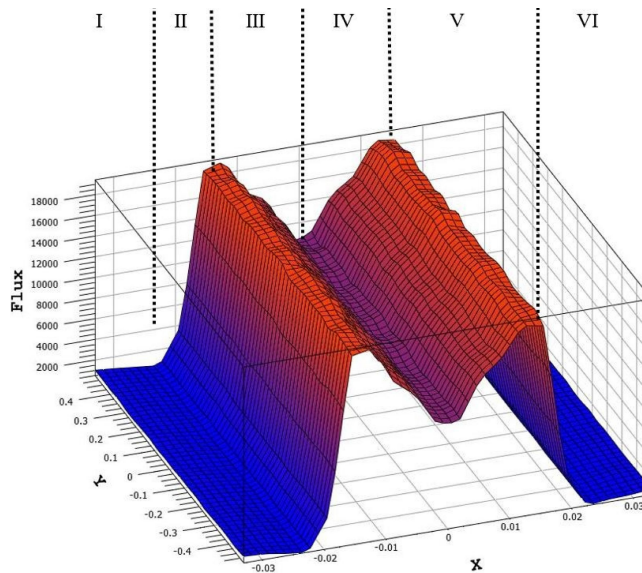


Figure 11: Surface plot of solar heat flux distribution along the absorber tube periphery.

the curve can be divided into six parts for ease of explanation of heat flux variation. In the first part of curve depicted in Fig. 11, heat flux intensity is very low, since in this part, the absorber tube only receives DNI. This is clear from the graph representing the change in heat flux distribution with the absorber tube circumferential angle (Fig. 12b) and the scatter plot shown in Fig. 12a. In the second part, heat flux increases rapidly and reaches a peak of  $19.44 \text{ kW/m}^2$  at about  $112.5 \text{ deg}$  circumferential angles from the top of the tube, as shown in Fig. 12b, then decreases rapidly

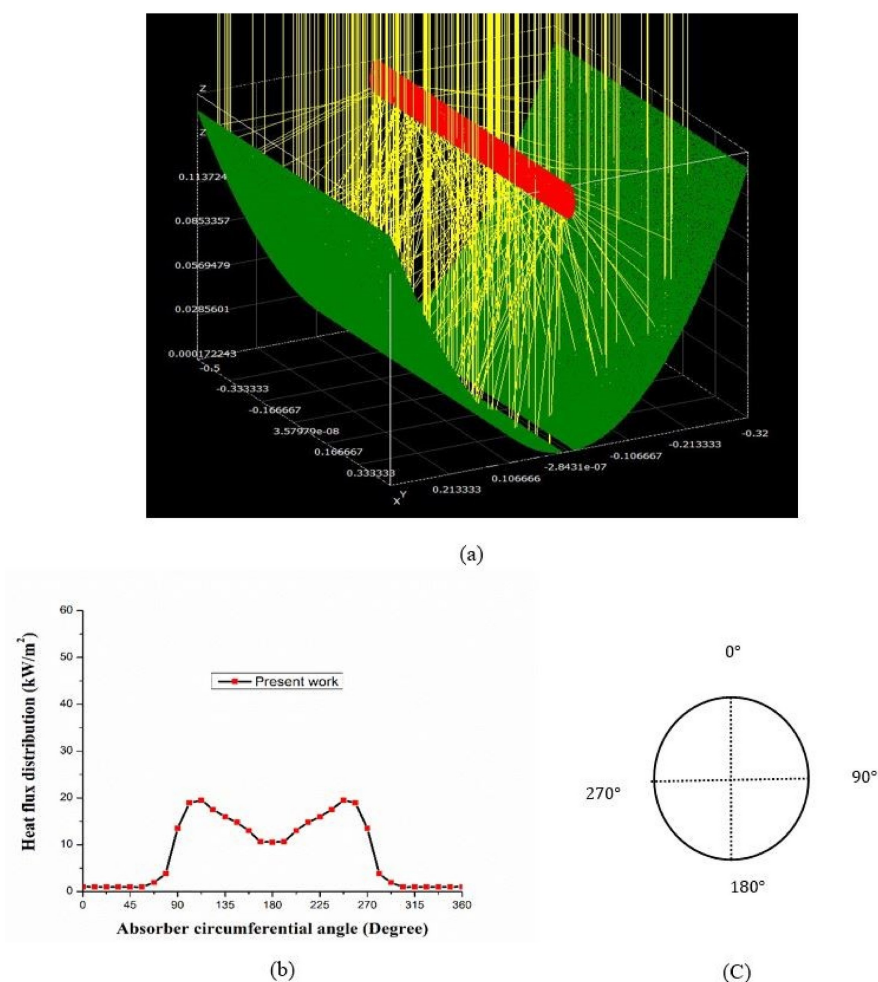


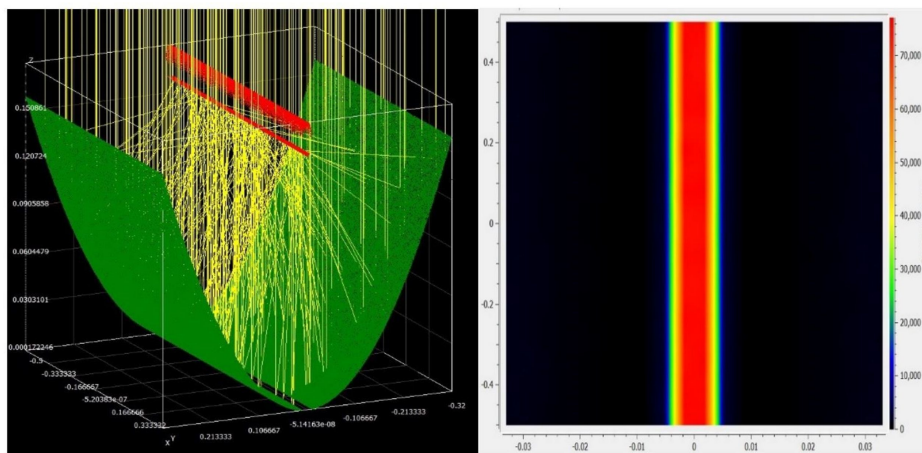
Figure 12: (a) Scatter plot for 90 deg rim angle, (b) heat flux vs. absorber circumferential angle, (c) absorber circumferential angle distribution.

and reaches a value of  $10.55 \text{ kW/m}^2$  at  $180 \text{ deg}$  in the third part due to a decrease in reflected heat flux, which can also be seen in the scatter plot in Fig. 12a. The curve is symmetrical about  $180 \text{ deg}$ , and the variation of heat flux in the next part exhibits the same characteristics as in the earlier one.

These CSHFD can be used as one of the boundary conditions in the CFD simulations for further thermal analysis.

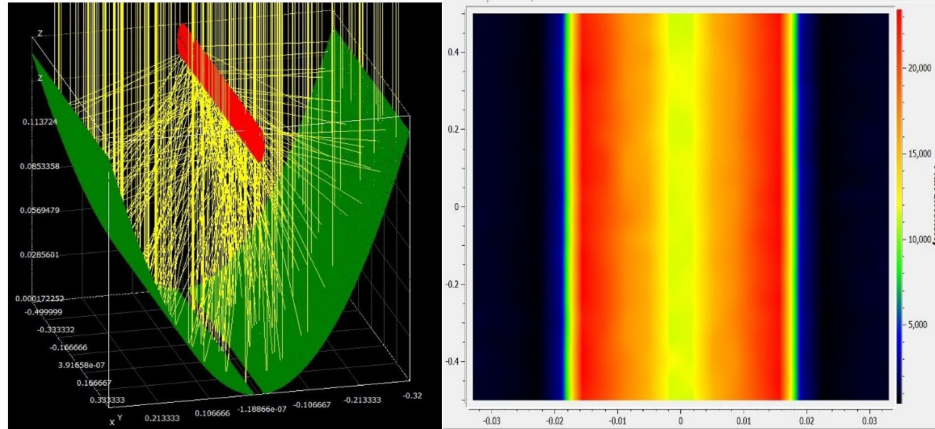
## 4.2 Receiver position error analysis

In this part, the numerical modelling software was used to investigate how the misalignment of the receiver along the optical axis affects the heat flux profile. For this analysis, the dimensional details have been incorporated from Table 4 without consideration of a slope or specularity error (i.e.,  $0.0001 \text{ mrad}$ ). As presented in Fig. 13, the centre of the absorber tube is shifted above the focal point of the parabolic trough by its outer radius ( $10.5 \text{ mm}$ ) in the first case (Fig. 13a), in which most of the reflected ray concentrates at the small bottom part of the absorber tube. In this case, the peak value of heat flux is  $76.95 \text{ kW/m}^2$ , i.e., almost 77 times DNI ( $1 \text{ kW/m}^2$ ) which is very high, and will increase CTG in the absorber tube. The second is the case when the absorber tube is concentric with the focal point (Fig. 13b). This is the ideal case, where the peak value of

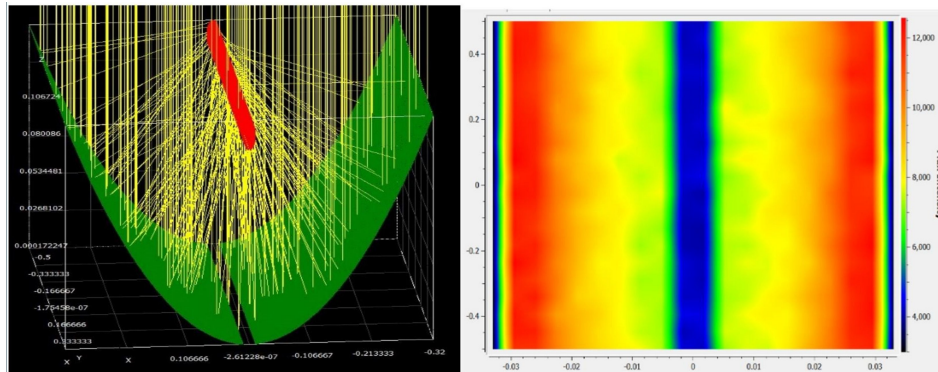


(a) Scatter plot and contour plot for absorber tube with the centre shifted by  $10.5 \text{ mm}$  above the focal point

Figure 13: For caption see next page.



(b) Scatter plot and contour plot for absorber tube concentric with the focal point



(c) Scatter plot and contour plot for absorber tube with the centre shifted by 10.5 mm below the focal point

Figure 13: Effect of receiver position misalignment along the optical axis on the heat flux profile.

heat flux is  $23.5 \text{ kW/m}^2$ , and the average value of heat flux is  $9.32 \text{ kW/m}^2$ , which is greater than the average value of  $8.17 \text{ kW/m}^2$  for the first case and  $8.16 \text{ kW/m}^2$  for the third one. The third case deals with the centre of the absorber tube being below the focal point by 10.5 mm (Fig. 13c). In this case, the absorber tube receives a poor value of peak heat flux ( $12.57 \text{ kW/m}^2$ ).

The above discussion reveals that the heat flux density is significantly affected by receiver misalignment along the optical axis.

### 4.3 Validation of numerical modelling results

For the validation of the present simulation work in SolTrace, the obtained outcome was compared with Jeter's result [10]. In his paper, the parameter local concentration ratio (LCR) is discussed [5]:

$$\text{LCR} = \frac{q}{\text{DNI}}, \quad (8)$$

where  $q$  represents the local heat flux.

Jeter's result corresponds to the parameter of the solar energy generating system (SEGS), solar collector (LS2 – Luz system 2) used in Sandia National Laboratories. Numerical simulation was carried out at the same geometrical dimensions, and optical and material properties as presented in [10] with normal irradiance, 90 deg rim angle and a uniform sun of 0.0075 mrad angular radius. The simulation results of LCR distribution at the cross-section of the absorber outer surface compared with those reported by Jeter are shown in Fig. 14. The comparison shows that the predictions agree well with Jeter's results, which also proves that the MCRT method used in the present work is viable and the numerical results are reliable.

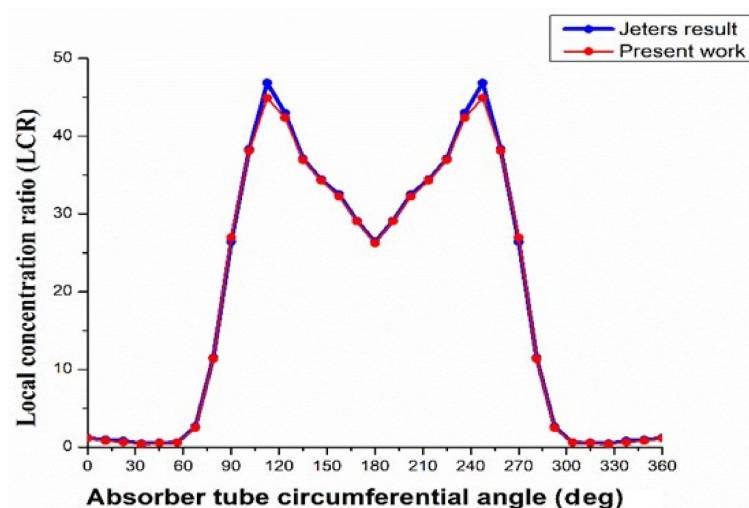


Figure 14: The LCR distribution – comparison between the present study and Jeter's results.

## 4.4 Sensitivity analysis

### 4.4.1 Influence of rim angle on the peak heat flux

The variation of the peak value of heat flux with the rim angle around the absorber tube periphery is shown in Fig. 15. Within the 30- to 130-degree rim angle, the peak value of heat flux is very large at 30 deg, with a poor value for peak heat flux at 130 deg. The peak value of heat flux for the rim angle varies little in the optimum range (70–110 deg).

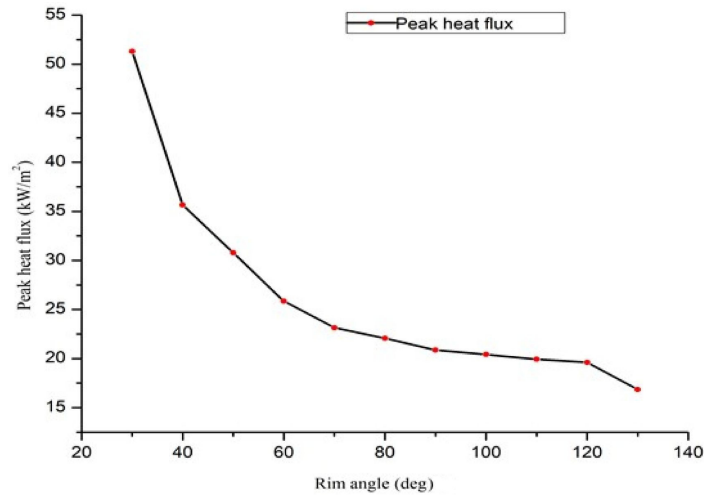


Figure 15: Peak heat flux *vs.* rim angle.

### 4.4.2 Heat flux variation along the receiver circumference for three different rim angles

The heat flux distributions along the absorber circumference for three different rim angles, namely 30 deg, 90 deg, and 130 deg, are compared in Fig. 16. Due to concentrated heat flux in a relatively small region of the absorber tube, a larger spike in the peak value of heat flux can be observed with a smaller rim angle of 30 deg. A poor value of peak and average heat flux is found for the relatively larger rim angle of 130 deg, while an acceptable range of peak heat flux and an optimum average heat flux is observed for the 90 deg rim angle. The heat flux profile distribution for different rim angles have been discussed in more detail in Section 2.1.

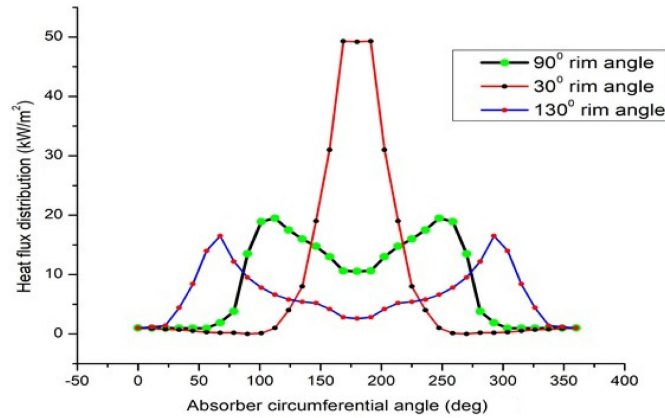


Figure 16: Comparison of heat flux profile along the absorber circumferential angle for different rim angles.

#### 4.4.3 Effect of absorber tube outer diameter on the heat flux profile

Figure 17 depicts the variation of heat flux distribution with the absorber tube's outer diameter. For this analysis, all parameters given in Tables 1 and 4 have been adopted, except for the receiver's outer diameter. The three different values of the absorber tube's outer diameter, 21 mm, 23 mm, and 25 mm

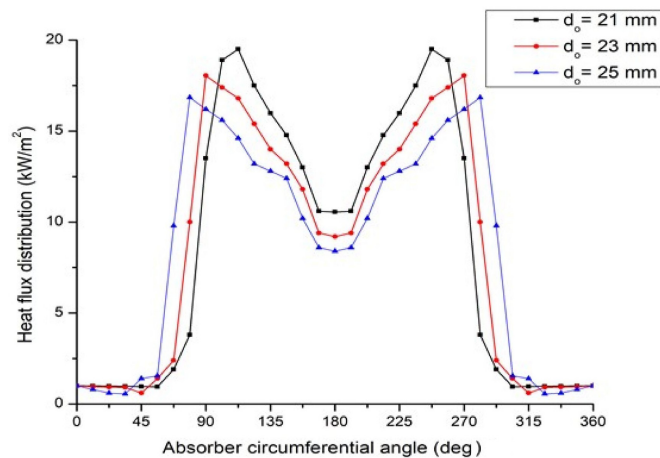


Figure 17: Variation of heat flux along absorber circumferential angle for different outer diameters of absorber tube.

25 mm, have been used while keeping the aperture width at 640 mm. As we know from Eq. (7), the concentration ratio depends on the width of an aperture as well as the outer diameter of the absorber tube. As the outer diameter increases, the concentration ratio decreases, resulting in a decrease in the value of heat flux intensity.

## 5 Conclusion

The present work focus on the geometrical optimization and optical analysis of a novel small-sized PTC based on the analysis of heat flux distribution around the circumference of the absorber tube using a ray tracing software called SolTrace. The outcome of this study can be summarised as follows:

- Heat flux distribution analysis was carried out for different values of rim angle within 30–130 deg, and an optimized rim angle of 90 deg was obtained on the basis of the optimum value of average heat flux and an acceptable range of peak heat flux to obtain the maximum collection of solar heat flux for a non-ideal concentrator. Also, the determined optimum rim angle falls within a range of values obtained by other researchers in the literature, which proves the Monte Carlo ray tracing method used in the present work is viable and the numerical results are reliable.
- Ray-intersection plots, contour plots and surface plots were provided. Also, the peak and average values of heat flux were presented for the different values of rim angle 30–130 deg, with a gap of 10 deg.
- An experimental model of a small-sized parabolic trough collector was designed and fabricated. The curvature of the parabolic trough was designed for an optimized value of rim angle 90 deg, and other parameters mentioned in Table 1. A laser light test of a small dimension parabolic trough was performed first for the feasibility test of the procedure before fabrication of the actual parabolic trough collector and was found successful. Also, the design methodology was presented through a flow chart.
- The heat flux around the circumference of the absorber tube is non-uniform in nature. The heat flux profile is found to be symmetrical about the bottommost point of the circular absorber tube. The maximum value of heat flux is found at the bottom part of the tube

(112.5 deg and 247.5 deg from the topmost point), and the heat flux decreases towards the top of the absorber tube due to only direct normal irradiation falling in this location.

- The effect of the receiver position error along the optical axis on the heat flux profile was analysed and found to be significant. A receiver with a centre 10.5 mm above and below the focal point of the parabolic trough increases peak heat flux by 227.44%, which is very large and decreases it by 46.8%, which is poor. A very large value of heat flux caused by concentrated rays at a very small area of absorber creates a greater value of circumferential temperature gradient, and a poor value of heat flux may decrease overall performance; hence, both large and poor values of peak heat flux are not recommended for the efficient functioning of a reliable before fabrication of the actual parabolic trough collector and was found successful.
- During the sensitivity analysis of the parabolic trough collector, it was observed that as the outer diameter of the absorber tube increases, while keeping the aperture width the same, the heat flux intensity around the circumference of the absorber tube decreases due to a decrease in the concentration ratio.
- The slope error has a significant impact on the uniformity of flux intensity and the peak heat flux at the focal point. When the slope error is low, the peak heat flux at the focal point of the trough is high. When the slope error is high, however, the peak heat flux and uniformity go down because the rays do not reflect as well off the concentrator.
- A comparison of the local concentration ratio distribution versus absorber tube circumferential angle was made between the present work and Jeter's result for the optimized value of rim angle 90 deg and the same geometrical configurations, and the profile of the curve is found to be very close. This proves that the Monte Carlo ray tracing method used in the present work is viable and the numerical results are reliable.
- The heat flux distribution profile along the absorber tube circumferential angle generated by using the Monte Carlo ray tracing method can be utilized as one of the boundary conditions in CFD.

Received 30 March 2023

## References

- [1] Abdulhamed A.J., Adam N.M., Ab-Kadir M.Z. A., Hairuddin A.A.: *Review of solar parabolic-trough collector geometrical and thermal analyses, performance, and applications*. *Renew. Sust. Energ. Rev.* **91**(2018), 822–831.
- [2] Stanek B., Bartela Ł., Węcel D., Rulik S.: *An experimental study on parabolic trough collector in simulated conditions by metal-halide solar radiation simulator*. *Arch. Thermodyn.* **43**(2022), 3, 47–61.
- [3] Wang Y., Potter D., Asselineau C.A., Corsi C., Wagner M., Caliot C., Piaud B., Blanco M., Kim J.S., Pye J.: *Verification of optical modelling of sunshape and surface slope error for concentrating solar power systems*. *Sol. Energy* **195**(2020), 461–474.
- [4] Mwesigye A., Bello-Ochende T., Meyer J.P.: *Minimum entropy generation due to heat transfer and fluid friction in a parabolic trough receiver with non-uniform heat flux at different rim angles and concentration ratios*. *Energy* **73**(2014), 606–617.
- [5] Donga R.K., Kumar S., Kumar A.: *Performance evaluation of parabolic trough collector with receiver position error*. *J. Therm. Eng.* **7**(2021), 1, 271–290.
- [6] Zhao D., Xu E., Wang Z., Yu Q., Xu L., Zhu L.: *Influences of installation and tracking errors on the optical performance of a solar parabolic trough collector*. *Renew. Energ.* **94**(2016), 197–212.
- [7] Treadwell G.W.: *Design considerations for parabolic-cylindrical solar collectors*. Sandia Laboratories Energ. Rep. **9**(1976), SAND-76-0082.
- [8] Treadwell G.W., Grandjean N.R.: *Systematic rotation and receiver location error effects on parabolic trough annual performance*. *Am. Soc. Mech. Eng.* **104**(1981), 345–348.
- [9] Ghomrassi A., Mhiri H., Bournot P.: *Numerical study and optimization of parabolic trough solar collector receiver tube*. *J. Sol. Energy Eng. Trans. ASME* **137**(2015), 5, SOL-15-1068.
- [10] Jeter S.M.: *Calculation of the concentrated flux density distribution in parabolic trough collectors by a semifinite formulation*. *Sol. Energy* **37**(1986), 5, 335–345.
- [11] Wang Y., Liu Q., Lei J., Jin H.: *Performance analysis of a parabolic trough solar collector with non-uniform solar flux conditions*. *Int. J. Heat Mass Transf.* **82**(2015), 236–249.
- [12] Cheng Z.D., He Y.L., Xiao J., Tao Y. B., Xu R.J.: *Three-dimensional numerical study of heat transfer characteristics in the receiver tube of parabolic trough solar collector*. *Int. Commun. Heat Mass Transf.* **37**(2010), 7, 782–787.
- [13] Dudley E., Kolb J., Mahoney A., Mancini T.R., Matthews C.W., Kearney D.: *Test results: SEGS LS-2 solar collector*. Sandia Nat. Lab. Rep. **140**(1994), SAND94-1884.
- [14] He Y.L., Xiao J., Cheng Z.D., Tao Y.B.: *A MCRT and FVM coupled simulation method for energy conversion process in parabolic trough solar collector*. *Renew. Energ.* **36**(2011), 3, 976–985.

- [15] Upadhyay B.H., Patel A.J., Sadasivuni K.K., Mistry J.M., Ramana P.V., Panchal H., Ponnamma D., Essa F.A.: *Design, development and techno economic analysis of novel parabolic trough collector for low-temperature water heating applications*. Case Stud. Therm. Eng. **26**(2021), 100978.
- [16] Günther M., Joemann M., Csambor S., Guizani A., Krüger D., Hirsch T.: *Parabolic trough technology*. In: Advanced CST Teaching Materials, Chap. 5, 51–43. DLR, Kassel 2011,
- [17] Upadhyay B.H., Patel A. J., Sadasivuni K. K., Mistry J. M., Ramana P.V., Panchal H., Ponnamma D., Essa F.A.: *Design, development and techno economic analysis of novel parabolic trough collector for low-temperature water heating applications*. Case Stud. Therm. Eng. **26**(2021), 100978.
- [18] Özcan A., Devocioğlu A G., Oruç V.: *Experimental and numerical analysis of a parabolic trough solar collector for water heating application*. Energ. Source. Part A Recover. Util. Environ. Eff. **44**(2022), 2, 4184–4203.
- [19] Bharti A., Mishra A., Paul B.: *Thermal performance analysis of small-sized solar parabolic trough collector using secondary reflectors*. Int. J. Sustain. Energ. **38**(2019), 10, 1002–1022.
- [20] Faheem M., Jizhan L., Akram M.W., Khan M.U., Yongphet P., Tayyab M., Awais M.: *Design optimization, fabrication, and performance evaluation of solar parabolic trough collector for domestic applications*. Energ. Source. Part A Recover. Util. Environ. Eff. (2020), 1–20.
- [21] Kalogirou S.A., Lloyd S., Ward J., Eleftheriou P.: *Design and performance characteristics of a parabolic-trough solar-collector system*. Appl. Energ. **47**(1994), 4, 341–354.
- [22] Menbari A., Alemrajabi A.A., Rezaei A.: *Experimental investigation of thermal performance for direct absorption solar parabolic trough collector (DASPTC) based on binary nanofluids*. Exp. Therm. Fluid Sci. **80**(2017), 218–227.
- [23] Price H., Lüpfert E., Kearney D., Zarza E, Cohen G., Gee R., Mahoney R.: *Advances in parabolic trough solar power technology*. J. Sol. Energy Eng. Trans. ASME **124**(2002), 2, 109–125.
- [24] Sukhatme S.P., Nayak J.K.: *Solar Energy Principles of Thermal Collection and Storage*. McGraw-Hill, New Delhi 2008.
- [25] Duffie J.A., Beckman W.A., McGowan J.: *Solar engineering of thermal processes*. Am. J. Phys. **53**(1985), 382–382.
- [26] Collares-Pereira M., Gordon J.M., Rabl A., Winston R.: *High concentration two-stage optics for parabolic trough solar collectors with tubular absorber and large rim angle*. Sol. Energy **47**(1991), 6, 457–466.
- [27] Ceylan I., Ergun A.: *Thermodynamic analysis of a new design of temperature controlled parabolic trough collector*. Energ. Convers. Manag. **74**(2013), 505–510.
- [28] <http://mscir.tripod.com/parabola/> (accessed 15 Aug. 2022).
- [29] Wendelin T.: *Soltrace: A new optical modeling tool for concentrating solar optics*. Int. Sol. Energy Conf. (2003), 253–260.
- [30] SolTrace optical modelling software, *SolTrace v.2012.7.9*. <http://www.nrel.gov/csp/soltrace/> (accessed 20 Oct. 2022).